Joint Special Interest Group meeting between euspen and ASPE
Advancing Precision in Additive Manufacturing
TU Berlin, Germany, October 2025
www.euspen.eu

Influence of process parameters on the quality of 316l stainless steel components fabricated by metal Fused Filament Fabrication

J. Polte[1, 2], E. Uhlmann[1, 2], A. Myrtaj[1*], S. Bode[1], T. Naderi[1], C. Schmiedel[2]

[1] *Institute for Machine Tools and Factory Management IWF, Technische Universität Berlin, Germany*
[2] *Fraunhofer Institute for Production Systems and Design Technology IPK, Germany*

**a.myrtaj@tu-berlin.de*

Abstract

The use of Fused Filament Fabrication for the production of metallic components requires comprehensive knowledge of the influence of processing parameters on part quality and reproducibility. Although the mechanical properties and microstructural behavior of metal-polymer composite filaments have been widely studied, systematic investigations focusing explicitly on simple cubic geometries to isolate parameter-induced effects remain limited. This study systematically evaluates the influence of layer thickness, nozzle temperature, and print speed on the dimensional accuracy, shrinkage, and density of BASF Ultrafuse 316L stainless steel parts fabricated on a Prusa MK4 system. A full factorial design of experiments was implemented, yielding a dataset of eighty-one specimens. Analyses after debinding and sintering reveal distinct correlations between printing parameters and both part shrinkage and density. The results provide baseline data that enhance the understanding of parameter-process-property relationships in metal-based Fused Filament Fabrication and offer practical guidance for the reliable fabrication of 316L stainless steel components with standard FFF equipment.

keywords: Metal Fused Filament Fabrication, Ultrafuse 316L, Parameter Study

1 Introduction

Metal Fused Filament Fabrication (FFF) has gained increasing attention as a cost-efficient and accessible technique for the production of metallic components, especially for users seeking alternatives to the high investment and process complexity associated with powder bed fusion (PBF-LB/M) or directed energy deposition (DED) methods [1]. The process involves the use of composite filaments in which stainless steel powder is embedded within a polymer binder matrix. After the initial shaping by extrusion, the printed parts undergo debinding and sintering to achieve dense metallic structures suitable for a range of applications. Compared to established metal additive manufacturing technologies, metal FFF simplifies material handling, reduces equipment requirements, and supports the fabrication of complex geometries [2, 3, 4]. However, the final quality of FFF-manufactured metal components depends on the entire process chain. Material properties including density, shrinkage, porosity, and mechanical strength are sensitive to the control of process parameters throughout extrusion, debinding, and sintering [5, 6]. Although the practical significance of metal FFF is recognized, systematic investigations addressing process parameter optimization remain relatively scarce, particularly for desktop printing platforms and simple geometric samples. This study focuses on the fabrication of metallic parts using Ultrafuse 316L with a Prusa MK4 FFF-printer from PRUSA RESEARCH A.S., CZECH REPUBLIC. The objective is to identify reliable process windows and to provide reference data that support reproducible results for research and industrial practice. In this context, the findings contribute to a broader understanding of the relationships between process conditions and the resulting part properties in metal FFF.

2 Materials and methods

2.1 Material and Printing Parameters

The material used in this study was the Ultrafuse 316L by BASF SE, LUDWIGSHAFEN AM RHEIN, GERMANY filament. This composite consists predominantly of approximately 90 wt.% AISI 316L stainless steel powder integrated into a polymeric binder matrix composed of polyoxymethylene (POM) and polyethylene (PE) [3]. The filament was supplied with a diameter of $D_F = 1.75$ mm. For the evaluation of suitable process conditions, three key printing parameters were identified: layer thickness d_S, nozzle temperature τ_{nozzle}, and printing speed v_D. These parameters were selected based on their strong documented influence on densification, dimensional accuracy, and mechanical performance of FFF-fabricated metallic parts, as established in both the technical literature and the recommendations provided by the filament manufacturer. Each of these variables was examined at three levels, which are listed in Table 1.

Table 1 Investigated printing parameters and their levels

Parameter	Level 1	Level 2	Level 3
Layer thickness d_S [mm]	0.1	0.2	0.3
Nozzle Temperature τ_{nozzle} [°C]	230	240	250
Printing Speed v_D [mm/s]	15	30	40

To systematically investigate the effects and possible interactions of the chosen process parameters, a full factorial

experimental design was applied. This approach yielded 27 parameter combinations, derived from the variation of layer thickness d_S, nozzle temperature τ_{nozzle}, and printing speed v_D at three levels each. For every combination, three specimens were printed in order to account for process variability, which resulted in a total of 81 samples. This methodology permits robust statistical analysis and enhances the reliability of the results. All other process parameters were kept constant throughout the study. The build plate temperature was set to τ_B = 100 °C, the infill density at In_ρ = 100 % and the extrusion multiplier at EM = 1.15. For all prints, a linear infill pattern was applied with a raster angle of ϕ = ±45 °, two perimeters, and an extrusion width of EW = 0.45 mm. During printing, the cooling fan was activated after the fourth layer, and the maximum volumetric flow rate was limited to MVS = 8 mm^3/s. Slicing and print preparation were conducted using PrusaSlicer 2.8.1 from PRUSA RESEARCH A.S., CZECH REPUBLIC, which provided consistent processing conditions for all parameter combinations. All specimens were fabricated using the FFF printer Prusa MK4, equipped with a d_{nozzle} = 0.4 mm hardened steel nozzle to ensure wear resistance during extrusion of the abrasive metal-filled filament.

2.2 Post-Processing

After printing, all green parts underwent a two-stage post-processing protocol consisting of catalytic debinding and subsequent sintering. The catalytic debinding was performed externally in the CD3045-HT-CE Oven from ELNIK SYSTEMS GMBH, EBHAUSEN, GERMANY, using nitric acid vapor at a temperature of τ_E = 120 °C. This step selectively removed the main polymer components of the binder system by chemical decomposition, leaving behind the brown part consisting primarily of metal powder held together by residual binder. Following debinding, the brown parts were sintered in the MIM3045 furnace from the same company, operated in a hydrogen atmosphere. The sintering process followed the manufacturer's recommended temperature profile, reaching a peak temperature of τ_S = 1,380 °C. During this thermal treatment, metallic particles were fused together through solid-state diffusion, leading to densification and the final consolidation of the metallic structure. The controlled furnace environment and ramp rates ensured uniform shrinkage and minimized distortion. Both debinding and sintering were carried out in accordance with the BASF processing guidelines for Ultrafuse 316L to ensure consistency and comparability of results across all samples. [4]

2.3 Analytical Methods and Test Setups

To comprehensively characterize the sintered parts, a range of analytical methods and test setups was employed. Dimensional accuracy was determined by measuring reference features in the x-, y-, and z-directions. Relative dimensional deviation δ was calculated as the percentage difference between the nominal L_n and measured L_g lengths. Shrinkage S was assessed as the percentage length change between the green and sintered parts in each direction. Density ρ and porosity ϕ were determined using the Archimedes method based on the principle for sinking solids, employing a precision scale PLS 1200–3A in combination with the density determination kit ALT-A02 from KERN & SOHN GMBH, BALINGEN, GERMANY. Surface roughness was measured using the Nanoscan 855 from HOMMEL ETAMIC GMBH, JENA, GERMANY, with a stylus tip radius of r_{tip} = 10 µm over a measurement length of l_m = 4 mm, divided into five segments. In cases where a mean roughness value of Ra ≤ 10 µm or a maximum height Rz ≤ 50 µm was measured, a repeated measurement was performed using a stylus tip radius of r_{tip} = 5 µm to achieve greater differentiation of fine surface features. The roughness was determined on the top, side, and bottom surfaces of representative samples. Vickers hardness testing was performed according to DIN EN ISO 6507-1 using a Dia Testor-2Rc universal hardness tester from OTTO WOLPERT-WERKE GMBH, GERMANY, at a test force of HV10. The test surface was prepared by mechanical grinding with silicon carbide papers. For each specimen, three indentations were made. Optical microscopy of the sintered parts was carried out with the digital microscope VHX-5000 from KEYENCE GMBH, NEU-ISENBURG, GERMANY, at magnifications of 100× and 200× to document the general surface quality and microstructure.

3 Results

3.1 Surface Analysis

All printed green parts were visually inspected prior to post-processing to evaluate surface quality, geometric consistency, and potential printing defects. Differences in surface texture, filament deposition, and layer alignment were observed across the 27 parameter combinations.

Figure 1 illustrates three representative specimens at different processing stages: Specimen V3 (d_{S1} = 0.1 mm, $\tau_{nozzle3}$ = 250 °C, v_{D1} = 15 mm/s), specimen V8 (d_{S1} = 0.1 mm, $\tau_{nozzle2}$ = 240 °C, v_{D3} = 40 mm/s), and V25 (d_{S3} = 0.3 mm, $\tau_{nozzle3}$ = 250 °C, v_{D2} = 30 mm/s). V3 exhibited the highest surface uniformity in the green state, featuring minimal visible defects and well-defined layer structures. Upon sintering, this specimen maintained a smooth, homogeneous surface with minimal residual artifacts, as confirmed by optical microscopy in Figure 2, which revealed uniform layer fusion and minimal porosity on both top and side surfaces.

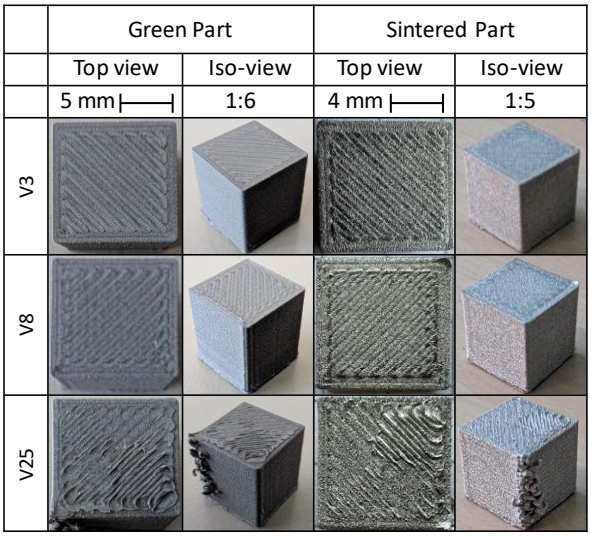

Figure 1 Surface comparison of green and sintered parts

Specimen V8, fabricated at a higher printing speed, displayed visible irregularities in filament deposition and a distinct Z-seam artifact already evident in the green state. Following the catalytic debinding and sintering processes, specimen V8 showed minor warping, particularly at corners, alongside pronounced stair-stepping effects due to insufficient material deposition consistency. Optical microscopy further highlighted these irregularities, capturing surface textures characterized by visible layer transitions and pronounced surface roughness.

Specimen V25, printed with the largest layer thickness d_{S3}, exhibited significant deposition irregularities and edge distortions at the green stage. These initial defects were notably exacerbated by subsequent sintering, leading to increased surface roughness, warping, and notable delamination at

corners and edges. Microscopic analysis of specimen V25 revealed discontinuities in interlayer bonding, elevated surface porosity, and structural irregularities that affected geometric fidelity. These observations demonstrate the persistent impact of initial printing conditions throughout the processing chain, emphasizing the sensitivity of surface quality and structural integrity to printing speed and layer thickness. Optimal parameters such as those used for specimen V3 yield stable and reliable outcomes, whereas elevated layer thicknesses and increased printing speeds consistently contribute to reduced dimensional accuracy, increased surface defects, and compromised structural quality.

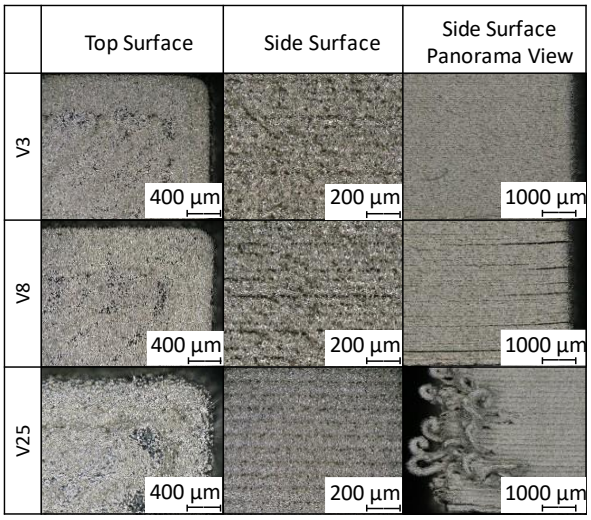

Figure 2 Microscopic surface views showing top and side surfaces

3.2 Dimensional Accuracy and Shrinkage

The dimensional accuracy of the green parts was assessed by measuring three reference edges along the x-, y-, and z-directions using a digital caliper. For each direction, the relative dimensional deviation δ was calculated with respect to the nominal length L_n = 10 mm. The analysis revealed the highest variability in the x-direction, with 0.1 % ≤ δ_x ≤ 3.3 % and a median value of $\delta_{x,med}$ = 1.18 %. In the y-direction, values were generally lower, with a median of $\delta_{y,med}$ = 0.54 %. The most consistent results were observed in the z-direction, with 0.02 % ≤ δ_z ≤ 1.3 % and a median of $\delta_{z,med}$ = 0.37 %. These results indicate the highest dimensional fidelity in the build direction and the greatest variation in the lateral plane, particularly along the x-axis. A multiple regression analysis was conducted to identify which printing parameters significantly influenced dimensional deviations. The results showed that the layer thickness d_S had a statistically significant effect on δ in all three directions, while the printing speed v_D affected δ_x and δ_y. In contrast, the nozzle temperature τ_{nozzle} had no statistically significant influence on dimensional accuracy. An interaction between d_S and v_D was found to be significant only in the z-direction, suggesting a combined influence on vertical resolution and deposition precision.

Following sintering, the total shrinkage S was evaluated as the percentage change in length between the green L_g and sintered L_s states. The theoretical reference values provided by the filament manufacturer were $S_{xy,th}$ = 16.6 % for the lateral plane and $S_{z,th}$ = 19.3 % for the build direction. Experimental shrinkage in the x-direction ranged from 16.2 % ≤ S_x ≤ 18.0 %, and in the y-direction from 16.1 % ≤ S_y ≤ 18.2 %. In the z-direction, greater variation was observed, confirming the expected anisotropic shrinkage due to the layer-wise build structure, with 18.5 % ≤ S_z ≤ 22.1 %. [4] A representative size comparison between green and sintered parts is shown in Figure 3.

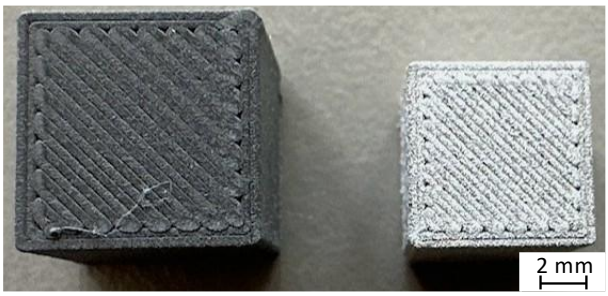

Figure 3 Visual comparison of green (left) and sintered part (right) (V16)

A second regression analysis identified statistically significant effects of all three parameters (d_S, v_D, τ_{nozzle}) on S_x. For S_y, d_S and τ_{nozzle} were significant, including their interactions with v_D. In the case of S_z, only d_S and v_D showed a significant linear influence; no interactions were observed. The lowest deviations from the reference shrinkage values were found at d_{S2} = 0.2 mm, $\tau_{nozzle2}$ = 240 °C, and v_{D2} = 30 mm/s, supporting this parameter set as a balanced trade-off between dimensional control and processing efficiency.

3.3 Density and Porosity

The density of the sintered specimens ρ_P was determined via the Archimedes method. Measured values ranged from 7.424 g/cm³ ≤ ρ_P ≤ 7.847 g/cm³. The highest density was achieved by specimen V3, closely matching the theoretical value ρ_{th} = 7.85 g/cm³ for AISI 316L [3]. Other specimens with high density included V5, V6, V8, and V15, all exceeding ρ_{P1} > 7.75 g/cm³. In contrast, the lowest densities were recorded for specimens V1, V13, V19, V20, and V21, all produced with either a low nozzle temperature ($\tau_{nozzle1}$ = 230 °C) or high layer thickness (d_{S3} = 0.3 mm). Their measured densities remained below ρ_{P2} < 7.58 g/cm³, indicating insufficient consolidation likely due to suboptimal process conditions or local inhomogeneities during debinding or sintering. A multiple regression analysis revealed that all three process parameters, layer thickness d_S, nozzle temperature τ_{nozzle}, and printing speed v_D, significantly influenced ρ_P, with τ_{nozzle} exerting the strongest individual effect. Interaction effects between v_D and τ_{nozzle}, as well as the three-way interaction among all parameters, were also statistically significant. The highest median densities were observed at d_{S1} = 0.1 mm, $\tau_{nozzle3}$ = 250 °C, and v_{D2} = 30 mm/s, which promoted dense and homogeneous filament deposition and sintering behavior. The porosity ϕ of the specimens, calculated indirectly via the measured density, was strongly inversely correlated with ρ_P. Total porosity ϕ_{tot} ranged from 0.48 % ≤ ϕ_{tot} ≤ 10.3 %. The lowest values were observed for specimens V3 and V8. The highest porosity occurred in V1 and V19, which were manufactured with low thermal input or increased layer thickness. A regression analysis on ϕ_{tot} showed that all three parameters significantly influenced porosity, with τ_{nozzle} again having the strongest individual effect. While two-way interactions were not significant, a three-way interaction among layer thickness d_S, nozzle temperature τ_{nozzle}, and printing speed v_D was statistically meaningful. The lowest porosity values were achieved at small layer thicknesses, intermediate to high printing speeds, and elevated nozzle temperatures.

3.4 Surface Roughness

Surface roughness of the sintered specimens was evaluated using tactile profilometry. Measurements were taken on three different surfaces of each part: the top surface, one vertical side,

and the bottom surface. The parameters analyzed included the arithmetic mean roughness Ra, maximum height Rz, total profile height Rt, and profile skewness Rsk. The bottom surfaces showed the lowest roughness values overall ranging from 1.4 µm ≤ Ra_b ≤ 3.9 µm, attributed to direct contact with the heated build plate. In contrast, the highest roughness was measured on the side surfaces ranging from 7.2 µm ≤ Ra_s ≤ 18.9 µm, due to the pronounced staircase effect inherent to the layer-wise fabrication in FFF. Top surfaces exhibited intermediate roughness levels, ranging from 4.0 µm ≤ Ra_t ≤ 14.1 µm. These were influenced by the deposition of the final solid infill and incomplete layer smoothing. A regression analysis revealed that the surface roughness of side walls was significantly affected by layer thickness d_S. Higher d_S values resulted in coarser step transitions and increased roughness, with average Ra values of Ra_1 = 8.63 µm at d_{S1}, Ra_2 = 11.54 µm at d_{S2}, and Ra_3 = 15.63 µm at d_{S3}. These trends were confirmed by Rz and Rt values, which also increased with thicker layers. In contrast, roughness on the bottom surface showed no significant dependence on process parameters and was excluded from further statistical analysis. For the top surface, both layer thickness d_S and printing speed v_D exhibited significant influence on Ra, including an interaction effect between the two. At lower d_S and moderate v_D, the smoothest top surfaces were achieved. However, Ra increased markedly when reached v_{D3} = 40 mm/s, with average values rising from Ra_4 = 6.41 µm for v_{D1} = 15 mm/s to Ra_5 = 8.49 µm. These results suggest that high printing speeds leads to less controlled material deposition and increased surface irregularities.

3.5 Vickers Hardness

The Vickers hardness (HV) of the sintered specimens was determined on polished cross-sections, with three to five indentations per sample. The hardness values ranged from 83 ≤ HV_t ≤ 122, falling below the reference value of HV_{th} = 128 specified in the BASF guidelines for Ultrafuse 316L [3]. The highest hardness values were measured for specimens V1, V2, V3, and V5, with results exceeding HV_1 = 119 and showing low variability. The lowest values were recorded for V21, V24, V25, and V26, all produced under conditions involving either reduced thermal input or increased layer thickness, with values ranging from 83 ≤ HV_2 ≤ 86. These outcomes indicate differences in microstructural consolidation resulting from the applied process settings. Specimens V10, V12, V18, and V19, fabricated using either intermediate or high layer thickness d_S, exhibited high standard deviations in hardness measurements, which may be attributed to local inhomogeneities or the presence of internal porosity. In these cases, additional indentations were performed to improve statistical robustness. Regression analysis revealed a significant influence of the layer thickness d_S on hardness. Thinner layers yielded higher and more consistent hardness values, while an increase in d_S was associated with lower HV values and broader variability. Neither printing speed v_D nor nozzle temperature τ_{nozzle} showed statistically significant effects on the measured hardness. No meaningful interaction effects between parameters were identified. These results indicate that the mechanical integrity of FFF-fabricated metal parts is primarily governed by the inter-layer bonding and porosity distribution influenced by layer height. Compared to other studies using Ultrafuse 316L, the values reported here are within the expected range for FFF-processed samples sintered in hydrogen atmospheres. However, they remain lower than those achieved in processes such as PBF-LB/M or DED, which generally yield finer microstructures and reduced porosity. While the maximum hardness measured in this study reached HV_{max} = 122, higher values have been reported in the literature for specimens fabricated using the same filament under different post-processing environments. For example, sintering under argon or vacuum atmospheres has yielded values above HV_a > 130 and, in some cases, up to HV_v = 220 [7, 8]. This highlights the sensitivity of mechanical properties to processing conditions and the need for precise control of both printing and post-processing stages.

4 Conclusion

This study systematically evaluated the influence of layer thickness d_S, nozzle temperature τ_{nozzle}, and printing speed v_D on the dimensional accuracy, shrinkage S, density ρ, surface roughness, porosity, and Vickers hardness of 316L stainless steel components produced by metal-based FFF using Ultrafuse 316L filament. A total of 81 specimens were manufactured under 27 parameter combinations using a full factorial experimental design. The results showed that all three process parameters significantly affected part quality, with layer thickness d_S having the most pronounced and consistent influence. Lower layer heights (d_{S1} = 0.1 mm) led to improved surface finish, higher density, reduced porosity, and increased hardness. Nozzle temperature τ_{nozzle} influenced densification and porosity, while printing speed v_D affected dimensional accuracy and surface topography. Interaction effects between the parameters were observed, particularly for shrinkage and porosity. Among all specimens, V3 (d_{S1} = 0.1 mm, v_{D1} = 15 mm/s, $\tau_{nozzle3}$ = 250 °C) achieved the most favorable results, combining high density, minimal porosity, low surface roughness, and the highest hardness value of HV_{max} = 122. By contrast, samples with higher layer thickness and suboptimal thermal input, such as V19 (d_{S3} = 0.3 mm, v_{D1} = 15 mm/s, $\tau_{nozzle1}$ = 230 °C), exhibited poor dimensional stability, reduced density, and increased surface defects. Although this work focused on simple cubic geometries, the findings provide practical reference data and serve as a foundation for process optimization in metal FFF. Based on the outcomes, the most promising parameter window lies in the range of 0.1 mm ≤ d_S ≤ 0.2 mm, 15 mm/s ≤ v_D ≤ 30 mm/s, and $\tau_{nozzle3}$ = 250 °C. These settings offer a viable balance between part quality and production efficiency when using standard FFF systems and commercially available metal filaments.

References

[1] Quarto, M.; Carminati, M.; D'Urso, G.: Density and shrinkage evaluation of AISI 316L parts printed via FDM process. *Materials and Manufacturing Processes* **36**, 1535 – 1543, 2021.

[2] Forward AM, BASF 3D Printing Solutions: User Guidelines; Ultrafuse 316L. Heidelberg, 2021.

[3] Forward AM, BASF 3D Printing Solutions: Technisches Datenblatt; Ultrafuse 316L. Heidelberg, 2022.

[4] Forward AM, BASF 3D Printing Solutions: Process Instructions; Ultrafuse 316L. Heidelberg, 2021.

[5] Thompson, Y.; Gonzalez-Gutierrez, J.; Kukla, C.; Felfer, P.: Fused filament fabrication, debinding and sintering as a low cost additive manufacturing method of 316L stainless steel. *Additive Manufacturing* **30**, 100861, 1 – 8, 2019.

[6] D'Andrea, D.: Additive manufacturing of AISI 316L stainless steel: A review. *Metals* **13**, 1370, 1 – 24, 2023.

[7] Carminati, M.; Quarto, M.; D'Urso, G.; Biardini, C.; Maccarini, M.: Mechanical characterization of AISI 316L samples printed using material extrusion. *Applied Sciences* **12**, 1433, 1 – 12, 2022.

[8] Raza, A.; Altaf, K.; Ahmad, F.; Hussain, G.; Alkahtani, M.; Wei, H.: Experimental study and characterisation of 316L stainless steel parts fabricated with metal fused filament fabrication. *Journal of Materials Research and Technology* **30**, 6686 – 6698, 2024.